

'Calving laws', 'sliding laws' and the stability of tidewater glaciers

Douglas I. BENN,^{1,2} Nicholas R.J. HULTON,³ Ruth H. MOTTRAM²

¹The University Centre in Svalbard (UNIS), Box 156, NO-9171 Longyearbyen, Norway
E-mail: Doug.Benn@unis.no

²School of Geography and Geosciences, University of St Andrews, St Andrews, Fife KY16 9AL, UK

³School of GeoSciences, University of Edinburgh, Drummond Street, Edinburgh EH8 9XP, UK

ABSTRACT. A new calving criterion is introduced, which predicts calving where the depth of surface crevasses equals ice height above sea level. Crevasse depth is calculated from strain rates, and terminus position and calving rate are therefore functions of ice velocity, strain rate, ice thickness and water depth. We couple the calving criterion with three 'sliding laws', in which velocity is controlled by (1) basal drag, (2) lateral drag and (3) a combination of the two. In model 1, velocities and strain rates are dependent on effective pressure, and hence ice thickness relative to water depth. Imposed thinning can lead to acceleration and terminus retreat, and ice shelves cannot form. In model 2, ice velocity is independent of changes in ice thickness unless accompanied by changes in surface gradient. Velocities are strongly dependent on channel width, and calving margins tend to stabilize at flow-unit widenings. Model 3 exhibits the combined characteristics of the other two models, and suggests that calving glaciers are sensitive to imposed thickness changes if basal drag provides most resistance to flow, but stable if most resistance is from lateral drag. Ice shelves can form if reduction of basal drag occurs over a sufficiently long spatial scale. In combination, the new calving criterion and the basal–lateral drag sliding function (model 3) can be used to simulate much of the observed spectrum of behaviour of calving glaciers, and present new opportunities to model ice-sheet response to climate change.

INTRODUCTION

Ice losses by calving exceed ablation by surface melting on the Antarctic and Greenland ice sheets, and calving is a significant ablation process on many other high- and mid-latitude ice masses. Because calving fluxes are strongly influenced by ice velocities, dynamic changes to outlet glaciers and ice streams can have a large effect on ice-sheet mass balance, providing a mechanism for rapid transfer of water to the oceans. Recently, calving glaciers in many parts of the world have undergone dramatic acceleration and retreat (e.g. Venteris, 1999; Thomas and others, 2004; Howat and others, 2005; Luckman and Murray, 2005; Rignot and Kanagaratnam, 2006), indicating a highly non-linear response to initial climatic forcing. Despite their important role in modulating the effects of climate change, the dynamics of calving glaciers are very poorly represented in existing ice-sheet models and constitute the largest source of uncertainty in predictions of future ice-sheet evolution. Development of a comprehensive general model of calving glacier dynamics is a formidable challenge involving some of the most stubborn problems in glaciology, including realistic parameterization of calving processes, the 'grounding-line problem' (e.g. Vieli and Payne, 2005) and the 'unresolved sliding problem' (Weertman, 1979). In this paper, we present a new framework for modelling tidewater glacier dynamics, using a new physically based calving criterion and alternative sliding functions. (Although not 'laws' in the physical sense, calving criteria and sliding functions are often referred to as such in the literature, and for convenience this convention is followed here.) Specifically we (1) assess the role of strain rates in calving processes and calving glacier dynamics, (2) explore feedback processes between strain rates, thinning, flow acceleration and terminus retreat, and (3) show how the new

framework can be used to represent a wide range of behaviours observed in tidewater glaciers and ice streams.

'CALVING LAWS'

Calving rate, U_C , is defined as the difference between ice velocity at the glacier terminus and glacier length change over time:

$$U_C = \bar{U}_T - \frac{\partial L}{\partial t}, \quad (1)$$

where \bar{U}_T is the depth-averaged velocity at the glacier terminus, L is the glacier length and t is time. Two contrasting approaches can be taken to solving Equation (1). In the first, a calving rate is estimated from independent variables, and changes in terminus position are determined from calving rate and ice velocity (e.g. Brown and others, 1982; Sikonja, 1982; Marshall and others, 2003; Siegert and Dowdeswell, 2004). Empirical relationships between calving rate and water depth, D_W , offer appealingly simple boundary conditions for calving in ice-sheet models:

$$U_C = a + bD_W. \quad (2)$$

The intercept a and gradient b differ for freshwater and tidewater calving glaciers (e.g. Funk and Röthlisberger, 1989; Warren, 1992), but also vary widely between regions (Haresign, 2004) and can even change through time for individual glaciers (Van der Veen, 1996).

The second approach inverts the problem, and determines calving losses from the ice velocity and changes in terminus position (Van der Veen, 1996, 2002). Using data from Columbia Glacier, Alaska, USA, Van der Veen (1996) found that at the calving front, ice thickness is consistently ~50 m greater than the flotation thickness, so that terminus

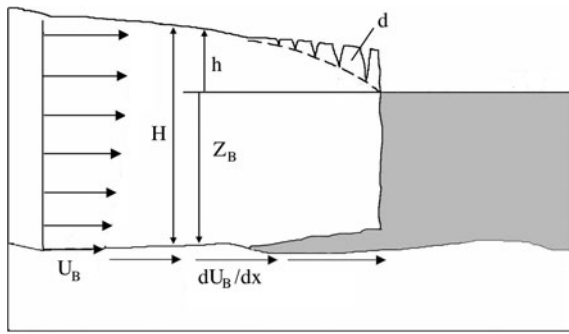


Fig. 1. Definition sketch of schematic calving terminus. The terminus may be either grounded (as shown) or floating, with any bed configuration.

position can be defined using a 'height-above-buoyancy' criterion:

$$H_T = \frac{\rho_W}{\rho_I} D_W + 50, \quad (3a)$$

where ρ_W and ρ_I are the densities of water and ice, respectively, and H_T is the ice thickness at the terminus (D_W and H_T in metres). Changes in ice thickness in the terminal zone will cause the glacier to advance or retreat until Equation (3a) is again satisfied. Vieli and others (2000, 2001) adopted a modified calving margin criterion, replacing the fixed height-above-buoyancy value with a factor q :

$$H_T = \frac{\rho_W}{\rho_I} (1 + q) D_W. \quad (3b)$$

As currently formulated, neither calving-rate functions nor terminus position criteria are based on physical principles, and both have major drawbacks. There is currently no means of deriving values for parameters a and b in Equation (2) from the physical configuration of the glacier (e.g. ice thickness, width) or other relevant variables, thus limiting its utility as a general calving law. Conversely, the Van der Veen and Vieli height-above-buoyancy criteria cannot represent all types of calving margin, because they do not permit ice shelves to form. This is a major limitation in models where the build-up of marine ice sheets is of interest.

To overcome the limitations of existing calving laws, we introduce a new calving criterion based on a simple model of crevasse formation. In nature, calving occurs following fracture propagation under local (and often complex) stress conditions, and it is neither possible nor desirable to attempt to model individual events. Instead, we assume that calving is triggered by the downward propagation of transverse surface crevasses, which open in response to down-glacier variations in flow speed (longitudinal strain rates). While doubtless this is a simplification of reality, we argue that this mechanism represents an important first-order control on the position of the calving front, on which other 'secondary' calving processes are superimposed.

We calculate crevasse depth following Nye (1957), by assuming that the base of a field of closely spaced crevasses lies at the depth where the longitudinal tensile strain rate (which tends to open crevasses) exactly balances creep closure resulting from the ice overburden pressure:

$$d = \frac{2}{\rho_I g} \left(\frac{\dot{\epsilon}_*}{A} \right)^{\frac{1}{n}}, \quad (4)$$

where g is gravitational acceleration, A and n are the flow-law parameters and $\dot{\epsilon}_*$ is the longitudinal strain rate ($\partial U / \partial x$) minus the threshold strain rate required for crevasse initiation ($\dot{\epsilon}_{\text{CRIT}}$). We use the Nye formulation in preference to the more rigorous linear elastic fracture mechanics (LEFM) approach of Smith (1976), Van der Veen (1998b) and Rist and others (1999), for three reasons. First, crevasse depths calculated using Van der Veen's (1998b) LEFM approach are highly sensitive to crevasse spacing, which is unknown a priori. Second, field data show that the Nye approach performs almost as well as that of Van der Veen at predicting observed crevasse depths (Mottram and Benn, unpublished data). Third, the much greater simplicity of the Nye formula makes it better suited for use in time-dependent ice-sheet models. Basal crevasses may also play a role in calving processes. However, theoretical analyses (Van der Veen, 1998a) indicate that the height of penetration is likely to be small except for very high longitudinal strain rates and very low basal effective pressures, so their role is ignored here. Equation (4) assumes plane strain, which is compatible with the two-dimensional flowline model adopted here (see below). Choice of an appropriate value of $\dot{\epsilon}_{\text{CRIT}}$ is difficult, because a wide range of values has been reported from laboratory and field studies (see Vaughan, 1993 for a review). Because our aim here is to outline the overall model structure, we adopt the simplifying assumption that $\dot{\epsilon}_{\text{CRIT}} = 0$ and

$$\dot{\epsilon}_* = \frac{\partial U}{\partial x}. \quad (5)$$

Crevasses that are partially or wholly filled with water will penetrate deeper than predicted by Equation (4) because the ice overburden pressure tending to close the crevasse is opposed by water pressure (Robin, 1974; Van der Veen, 1998a, b). Incorporating the effect of water pressure into Equation (4) yields:

$$d = \frac{2}{\rho_I g} \left[\left(\frac{\dot{\epsilon}_*}{A} \right)^{\frac{1}{n}} + (\rho_w g d_w) \right], \quad (6)$$

where d_w is the water depth in the crevasse. If the volume of water is fixed, d will have a stable value, but, if water is continually added to the crevasse, d will increase without limit and can eventually penetrate the full thickness of the glacier. Sustained water input can occur in response to surface melt or from supraglacial ponds (e.g. Scambos and others, 2000; Alley and others, 2005) or if a free connection exists between the crevasse and the proglacial water body, which is most likely if the crevasse is located close to the glacier margin. For present purposes, we assume that such a connection exists, so that surface crevasses will penetrate the full glacier thickness where they reach sea or lake level. In this case, the calving margin can be conveniently located where d equals the glacier 'freeboard' above sea level, h (Fig. 1):

$$x = L \quad \text{where} \quad d(x) = h(x), \quad (7)$$

where x is the horizontal coordinate parallel to glacier flow, positive downstream, L is glacier length and $h = H - D_W$.

The down-glacier velocity gradient, $\partial U / \partial x$, and the difference between ice thickness and water depth, h , are therefore considered to be the primary controls on glacier terminus position. The crevasse-depth calving criterion provides a simple physical explanation for the Van der Veen/Vieli height-above-buoyancy model, while allowing

ice shelves to form. Where velocity gradients are high, crevasses will penetrate to the waterline before the glacier reaches flotation, producing a grounded calving front. On the other hand, where there are only small longitudinal velocity gradients near the grounding line, an ice shelf may form.

'SLIDING LAWS'

The behaviour of calving glaciers depends critically on the ice velocity, for two reasons. First, ice velocity determines the rate at which ice is delivered to the calving front (Equation (1)), and is thus a primary control on calving flux. Second, longitudinal strain rate is the first derivative of velocity (Equation (5)), so down-glacier variations in velocity strongly influence both the terminus position (Equation (7)) and temporal changes in ice thickness by dynamic thinning. In this section we outline three alternative 'sliding laws', each of which has different implications for the location of the calving margin and glacier response to imposed thickness changes. We focus on flow along the centre line of an outlet glacier, with the x coordinate directed down-flow, and the z co-ordinate vertical, positive upward from sea or lake level. It is assumed that the shear stress components, τ_{xy} and τ_{yz} , the transverse deviatoric normal stress, σ'_{yy} , and the transverse velocity, V , are zero.

Appropriate functions for calculating basal motion, U_B (which we take to include all basal processes, including sliding in the narrow sense and deformation of subglacial sediment), depend on the forces resisting flow. The force-balance approach developed by Van der Veen and Whillans (1987) defines the relationship between driving and resisting stresses as:

$$\tau_D = \tau_B - \frac{\partial}{\partial y}(H\bar{R}_{xy}) - \frac{\partial}{\partial x}(H\bar{R}_{xx}), \quad (8)$$

where τ_D is the driving stress, the first term on the righthand side is basal drag, the second term is resistance to flow arising from lateral drag, and the third term is resistance arising from longitudinal stress gradients. In the results reported here, the longitudinal stress gradient term is neglected (cf. Van der Veen, 1999), and we focus on the role of basal and lateral drag in controlling the flow of calving glaciers.

Model 1 assumes that basal drag is the only non-zero resistance term:

$$\tau_B = \tau_D = \rho_l g H \frac{\partial h}{\partial x}. \quad (9)$$

This assumption underpins the widely used 'sliding law' introduced by Budd and others (1979):

$$U_B = k \tau_D^P P_E^{-Q}, \quad (10)$$

where k is a sliding rate factor, P_E is the effective pressure and P and Q are empirically determined exponents. Widely varying values of k , P and Q have been reported in the literature (e.g. Bindshadler, 1983; Raymond and Harrison, 1987; Iken and Truffer, 1997). To our knowledge, the only values determined for a tidewater glacier are those obtained for Columbia Glacier, Alaska, by Nick (2006): $k = 9.2 \times 10^6 \text{ m a}^{-1} \text{ Pa}^{0.5}$, $P = 3$ and $Q = 3.5$, and these are adopted here. The effective pressure is the difference between ice overburden pressure, $P_l = \rho_l g H$, and basal water pressure, P_W . For a calving glacier where basal water

flows towards the terminus, a minimum value for the basal water pressure is determined by the depth of the bed below sea level, Z_B . It is therefore useful to define the effective pressure in terms of this minimum value, plus an additional component ϕ associated with the subglacial transport and storage of meltwater:

$$P_E = \rho_l g H - (\rho_W g Z_B + \phi) \quad (11)$$

(e.g. Meier and Post, 1987; Van der Veen, 1999). In the simplest model case, ϕ can be set to zero (cf. Vieli and others, 2001), although this will tend to produce unrealistic velocity distributions, as discussed below. Values of ϕ can be modelled explicitly (cf. Flowers and Clarke, 2002), or prescribed using an assumed piezometric gradient.

In model 2, all of the driving stress is supported by drag at the lateral margins. Shear stress at the margins, τ_S , is related to the driving stress, τ_D , by a factor that varies with channel geometry. For a rectangular channel the relationship is:

$$\tau_S = \frac{W}{H} \tau_D. \quad (12)$$

This approximates the situation in ice shelves and some ice streams (Van der Veen, 1999). The centre-line velocity is calculated by integrating the flow law for ice from the flow-unit margins to the centre line:

$$U_B = \frac{2A}{n+1} \left(\frac{\tau_D}{H} \right)^n W^{n+1}, \quad (13)$$

where W is the flow-unit half-width. From the definition of τ_D (Equation (11)), this is equivalent to:

$$U_B = \frac{2A}{n+1} \left(\rho_l g \frac{\partial H}{\partial x} \right)^n W^{n+1}. \quad (13a)$$

Thus, velocity is independent of ice thickness, but if $n = 3$, centre-line velocity is proportional to the third power of the surface slope and the fourth power of the flow-unit width.

In model 3, resistance to flow is provided by a combination of basal and lateral drag. Theoretical sliding laws for this situation have been proposed by Raymond (1996) and Van der Veen and Whillans (1996). We derive a new sliding function by (1) scaling basal drag to the driving stress and basal water pressure and (2) using this value to derive a modified form of Equation (13). For step (1), we begin by assuming that $\tau_B = 0$ when $P_W = P_l$ and $\tau_B = \tau_D$ when $P_W = 0$. Variation of τ_B between these limits is then defined by:

$$\tau_B = \left(1 - \frac{P_W}{P_l} \right)^C \tau_D, \quad (14)$$

where C is a tuning parameter. In step (2), a sliding function is obtained by replacing τ_D in Equation (13) with the component of the driving stress that is not supported by basal drag,

$$U_B = \frac{2A}{n+1} \left(\frac{\tau_D - \tau_B}{H} \right)^n W^{n+1}. \quad (15)$$

This formulation implicitly assumes a rectangular cross-section, and that basal drag is constant across the bed. Equation (15) is similar to the dimensionless sliding function derived by Raymond (1996), but with the advantage that the relationship between basal drag and effective pressure can be easily varied using a single parameter C . Preliminary experiments with the Columbia Glacier dataset presented by Krimmel (2001) indicate that a good fit between modelled and observed velocities can be obtained when

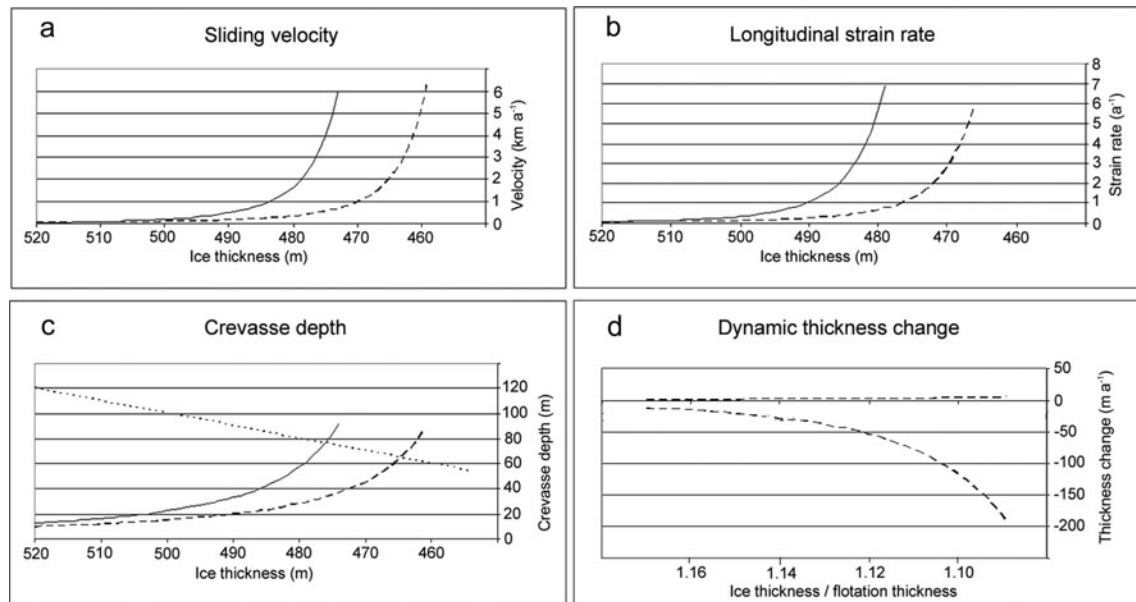


Fig. 2. Model 1: (a–c) relationships between ice thickness and (a) velocity, (b) longitudinal strain rate and (c) crevasse depth; and (d) relationship between normalized height above buoyancy and dynamic thickening rate. $Z_B = 400$ m; surface slope = 1.15° ; water density = 1030 kg m^{-3} (solid dark lines) and 1000 kg m^{-3} (dashed lines). The calving margin is located where the ice height above the waterline (dotted line in (c)) equals crevasse depth.

$C = 0.2$, and reasonable values are used for the piezometric gradient (see below).

The velocity at the ice surface is the sum of basal motion and the cumulative velocity, U_i , resulting from vertical shear in the ice. For fast-flowing calving glaciers, the creep component can be assumed to be small compared to basal sliding, and in the work presented here we assume that the calculated basal velocity, U_B , is equal to the vertically averaged ice velocity, U . It is useful, however, to consider the implications of the assumptions of the three flow models for the calculation of ice creep velocities. In model 1, the implicit assumption that the driving stress is equal to an opposing basal drag leads to the unrealistic result that vertical shear will occur even when the basal effective pressure is very small. Calculated creep velocities, therefore, will be increasingly unrealistic as flotation is approached. In model 2, basal drag is zero, so no vertical shear occurs. This contrast between models 1 and 2 highlights the difficulty of coupling sheet-flow and ice-shelf models across the grounding line: the mutually exclusive assumptions of the models preclude any smooth transition between them. Model 3 overcomes this problem by dealing with both grounded and floating ice within a single framework. The strain rate in simple shear is given by the constitutive relation:

$$\dot{\epsilon}_{xz} = A\tau_e^{n-1}\tau_{xz}, \quad (16)$$

where τ_e is the effective stress, and

$$\tau_{xz} = \frac{h-z}{H}\tau_B. \quad (17)$$

By scaling τ_{xz} to τ_B instead of τ_D , vertical shear strain will tend toward zero as basal drag vanishes, allowing a smooth transition between grounded and floating parts of the model domain. If it is assumed that $\tau_{xy} = \tau_{yz} = \sigma'_{yy} = 0$ and $\sigma'_{xx} + \sigma'_{zz} = 0$, the effective stress is given by:

$$2\tau_e^2 = 2\sigma_{xx}^2 + 2\tau_{xz}^2. \quad (18)$$

The longitudinal deviatoric stress, σ'_{xx} , is not known, but a first approximation can be obtained from the longitudinal strain rate derived from the basal velocity gradient. A consistent set of solutions for Equations (16), (18) and U_B can then be obtained iteratively.

COUPLING CALVING AND SLIDING LAWS

We now examine the behaviour of the crevasse-depth calving law coupled with the three alternative sliding laws (Equations (10), (13) and (15)), by analyzing how flow speed, terminus position and dynamic thinning rates respond to imposed changes in ice thickness and flow-unit width. Change in ice thickness through time is obtained from the continuity equation:

$$\frac{\partial H}{\partial t} = M - U\frac{\partial H}{\partial x} - H\frac{\partial U}{\partial x} - H\frac{\partial V}{\partial y}, \quad (19)$$

where the first term on the righthand side is the surface or basal mass balance (accumulation positive, ablation negative), the second term represents the advection of thicker ice from up-glacier (advective thickening), the third term is dynamic thinning (thickening) resulting from longitudinal stretching (shortening), and the fourth term is dynamic thinning (thickening) resulting from flow divergence (convergence) in the y (transverse) direction (on a flowline, the advective thickening term in the y direction is zero). By assuming that ice in a widening channel remains in contact with the sides, the transverse divergence term can be expressed in terms of the velocity in the x direction, U , and half-width, W :

$$\frac{\partial V}{\partial y} = \frac{U}{W}\frac{\partial W}{\partial x} \quad (20)$$

(Sanderson, 1979; Van der Veen, 1999).

When U is calculated using model 1, ice velocity increases as ice thickness decreases towards the flotation thickness. Velocities calculated from ice thickness, water

depth and surface slope values representative of the terminal zone of Columbia Glacier in 1988 (when fast flow was well established and terminus retreat was in progress) are shown in Figure 2a. In the example shown, it is assumed that $\phi = 0$ (Equation (11)), equivalent to a horizontal piezometric surface at sea level. As ice thickness decreases, modelled velocity increases non-linearly. The non-linear increase in velocity means that the longitudinal velocity gradient, $\partial U/\partial x$, also increases as ice becomes thinner (Fig. 2b), with the result that modelled crevasse depths also increase as the glacier thins towards the waterline (Fig. 2c). Because $\partial U/\partial x$ tends towards infinity as P_E approaches zero, the equality $d = h$ will always be met while the glacier is still grounded. Thus, the physically impossible solution to Equation (10) – a floating ice shelf with an infinite velocity – is precluded because the calving criterion predicts that crevasses will penetrate the full thickness of the glacier before flotation occurs. In the present example, the model predicts that the terminal ice cliff is 65–77 m high, and that the ice velocity at the terminus (and hence calving rate) is 2.2–3.2 km a⁻¹, depending on fjord water salinity. The modelled calving rate is lower than the observed value of ~ 5.4 km a⁻¹. There are several possible reasons for this discrepancy, including the unrealistic assumption that $\phi = 0$ throughout the glacier tongue (cf. Meier and others, 1994). Similar values for terminal ice cliff height and more realistic calving rates can be obtained using a piezometric gradient of 0.005 m m⁻¹. The impact of piezometric gradient on modelled velocities, strain rates and calving rates is discussed in greater detail below, with respect to model 3.

Modelled velocities, strain rates and crevasse depths are all greater for glaciers terminating in sea water ($\rho_W = 1030$ kg m⁻³) than fresh water ($\rho_W = 1000$ kg m⁻³), for any given ice thickness (Fig. 2). This is because a greater density difference between ice and the proglacial water body has a large effect on the maximum possible effective pressure at the glacier bed, and hence ice velocities (Van der Veen, 2002). For any given combination of ice thickness and water depth, greater amounts of ice will be delivered to a tidewater calving front than a freshwater one, explaining the oft-noted contrast in water-depth–calving-rate functions between marine and lake-terminating glaciers (e.g. Warren, 1992; Van der Veen, 1996, 2002).

When output from model 1 is inserted into the continuity equation (19), an interesting pattern emerges. Because ice velocity increases as ice approaches flotation, the advective thickening term increases down-glacier (Fig. 2d, upper curve). However, thinning in response to longitudinal stretching increases much more rapidly as ice thickness decreases (Fig. 2d, lower curve). For the 1988 Columbia Glacier terminus geometry, the continuity equation predicts strong dynamic thinning, increasing exponentially as the glacier approaches flotation. This provides a possible explanation for the observed rapid retreat of Columbia Glacier: an imposed thinning (due, for example, to increased melting) will trigger accelerated ice flow and dynamic thinning, which could then become a self-sustaining process. A dynamic thinning feedback will trigger terminus retreat because (1) as ice thickness decreases, it is increasingly likely that crevasses will penetrate down to the waterline, and (2) increased longitudinal strain rates result in deeper crevasses. In combination, these two effects will cause the glacier terminus to retreat up-glacier until it is able to stabilize in shallower water. Any tendency to dynamic

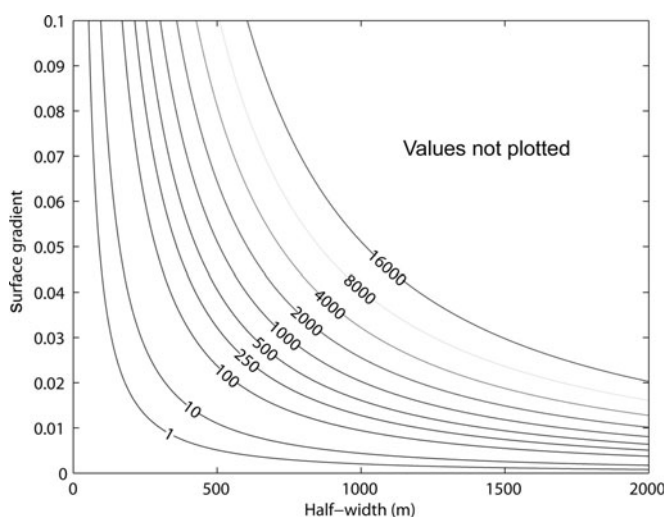


Fig. 3. Model 2: centre-line velocity as a function of channel half-width, W , and surface gradient.

thinning will be increased if the channel width increases downstream, and damped if it decreases due to the lateral divergence term in the continuity equation (Equations (19) and (20)). Thus, despite its simple formulation, model 1 successfully exhibits the well-known tendency for calving glaciers to stabilize at 'pinning points' (e.g. narrow or shallow sections of a fjord), and to retreat rapidly between pinning points during periods of negative mass balance (cf. Vieli and others, 2000, 2001). The model also predicts that sensitivity to imposed thinning is stronger for tidewater than freshwater-terminating glaciers.

In model 2, where ice velocity is controlled entirely by lateral drag, glacier response to changes in ice thickness and channel width contrasts markedly with model 1. Imposed glacier thinning will not result in flow acceleration unless thinning is also associated with an increase in surface slope. The lack of a direct relationship between ice thickness and velocity means that ice can become fully buoyant without experiencing the high longitudinal velocity gradients required for crevasse propagation and calving failure. In contrast, ice velocity is proportional to the third power of surface slope and the fourth power of channel width (for $n = 3$; Fig. 3). Thus, flow acceleration will occur if the glacier steepens, and particularly strong acceleration will occur at channel widenings. Where W increases, accelerating flow leads to longitudinal stretching, so that crevasses are likely to penetrate to the waterline and trigger calving failure at such locations. This sensitivity to channel width is much stronger than in model 1, in which velocity is influenced by W only through the lateral divergence term in the continuity equation. This feature of model 2 provides the most likely explanation for the tendency for tidewater glacier and ice-shelf margins to be located at topographic widenings.

In model 3, sliding velocity is sensitive to changes in both ice thickness relative to water depth and channel width. Figure 4 illustrates the behaviour of the combined basal–lateral-drag 'sliding law' (Equation (15)) using ice-thickness and driving-stress values representative of the 1988 Columbia Glacier geometry, and $C = 0.2$. The half-width of the glacier terminus was ~ 2.5 km at that time, and it can be seen that the model predicts velocities in the correct range

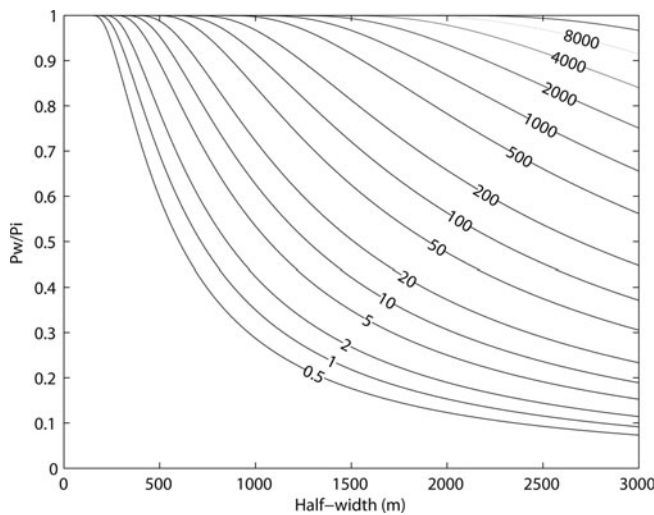


Fig. 4. Model 3: centre-line velocity as a function of P_w/P_i and $W\tau_D = 95$ kPa, $H = 480$ m, $C = 0.22$ (values representative of the marginal zone of Columbia Glacier in 1988).

($\sim 5 \text{ km a}^{-1}$) when $P_w/P_i \approx 0.95$. Like model 1, velocities increase non-linearly as basal water pressure approaches the ice pressure (i.e. as basal drag tends towards zero), but unlike model 1 velocities have a finite value when flotation occurs. This means that calving will not necessarily occur before the terminus goes afloat (as in model 1), but will depend on the spatial scale over which τ_B vanishes. If basal drag diminishes rapidly as the ice approaches flotation, calving will occur while the ice is still grounded, whereas if the transition from high to low values of τ_B occurs over a long distance, high longitudinal strain rates are avoided and an ice shelf can form. Thus, lateral drag potentially has a stabilizing effect on calving glacier termini.

Modelled velocity gradients, crevasse depths and dynamic thickening rates for the Columbia Glacier example are shown in Figure 5. Figure 5a, c and e show results for $\phi = 0$ (horizontal piezometric surface at sea level), and Figure 5b, d and f show results for the more realistic situation of ϕ rising up-glacier (equivalent to a piezometric gradient of 0.012, chosen to achieve the best fit with the observed velocities). Allowing ϕ to rise up-glacier has the effect of reducing modelled longitudinal strain rates and crevasse depths relative to the $\phi = 0$ case. Both model runs over-predict glacier length, and calving does not occur until the glacier is within ~ 0.98 of flotation. In physical terms, this over-prediction may reflect deficiencies in the crevasse depth model, or the omission of important factors such as longitudinal stress gradients, surface meltwater entering crevasses, or 'secondary' calving processes associated with longitudinal stress gradients in the immediate vicinity of the ice front (cf. O'Neel and others, 2003). Despite these difficulties, however, the model performs remarkably well at predicting the approximate position of the calving margin. Figure 5e and f show calculated dynamic thinning rates for the two modelled cases. The thinning tendency is greater for $\phi = 0$, because of higher longitudinal stretching rates, but in both cases the model indicates that the glacier terminus is unstable and 'locked into' a self-reinforcing thinning process. We propose that this modelled behaviour captures the fundamental process responsible for the observed behaviour of Columbia and other tidewater glaciers: an

imposed thinning triggers a positive feedback between acceleration, dynamic thinning and calving retreat. Importantly, the model predicts that this feedback is much less likely to operate where surface gradients are low, basal drag diminishes over large distances, and lateral drag provides most resistance in the vicinity of the grounding line. Thus, model 3 suggests that water-terminating glaciers will tend to be potentially unstable if basal drag provides most resistance to flow in the terminal zone, and stable if most resistance is provided by lateral drag.

Centre-line velocities calculated from Equation (15) are also highly sensitive to changes in glacier width (Fig. 4). High longitudinal strain rates and deep crevasses will therefore occur at widenings of fjords and embayments, making it likely that calving margins will be located in such places. Conversely, where W decreases down-glacier, velocity will decrease for any given value of the driving stress. Of course, continuity requires that dynamic thickening must occur if W and U both decrease; this tendency means that the driving stress will increase until sufficient ice is discharged through the constriction.

In its present form, model 3 does not include longitudinal stress gradients. Higher-order modelling by Payne and others (2004) and Hindmarsh (2006) suggests that this term in the force balance plays an important role in modulating the transition between equilibrium states, and further work is required to establish where and when the assumptions of model 3 are appropriate. Nevertheless, model 3 represents a considerable improvement on existing methods of representing calving processes and their relationship with ice dynamics, and has the potential to explain and simulate many elements of the observed behaviour of calving glaciers.

CONCLUSIONS

A simple physically based calving law, which defines the position of the glacier terminus as the point where crevasse depth equals the ice 'freeboard' above sea level, provides a more flexible and robust marine boundary condition for ice-sheet models than existing calving laws.

Terminus retreat can be triggered either by increases in longitudinal strain rates (which cause deeper crevasses), or by decreases in ice thickness (which increase the likelihood that crevasses will reach the waterline).

Modelled glacier dynamics depends critically on the choice of sliding law. Where sliding velocity is inversely proportional to effective pressure, any imposed thinning on a calving glacier will lead to ice acceleration and retreat of the calving front because effective pressure is influenced by water depth. Feedbacks between ice thickness, sliding velocity and dynamic thinning provide a powerful means of amplifying initial signals. Increased melting in the terminal zone can trigger acceleration, thinning and terminus retreat. This scenario was modelled by Vieli and others (2001) and suggests that, where resistance to flow is mainly from basal drag, calving glaciers are highly sensitive to external triggers, because of the dynamical instability of the system as ice approaches flotation.

In contrast, where all resistance to flow is provided by lateral drag, ice velocity is insensitive to imposed thickness changes, unless these are associated with changes in ice surface gradient. The position of the calving front is strongly influenced by topography, because ice velocity is proportional to the fourth power of channel half-width. Channel

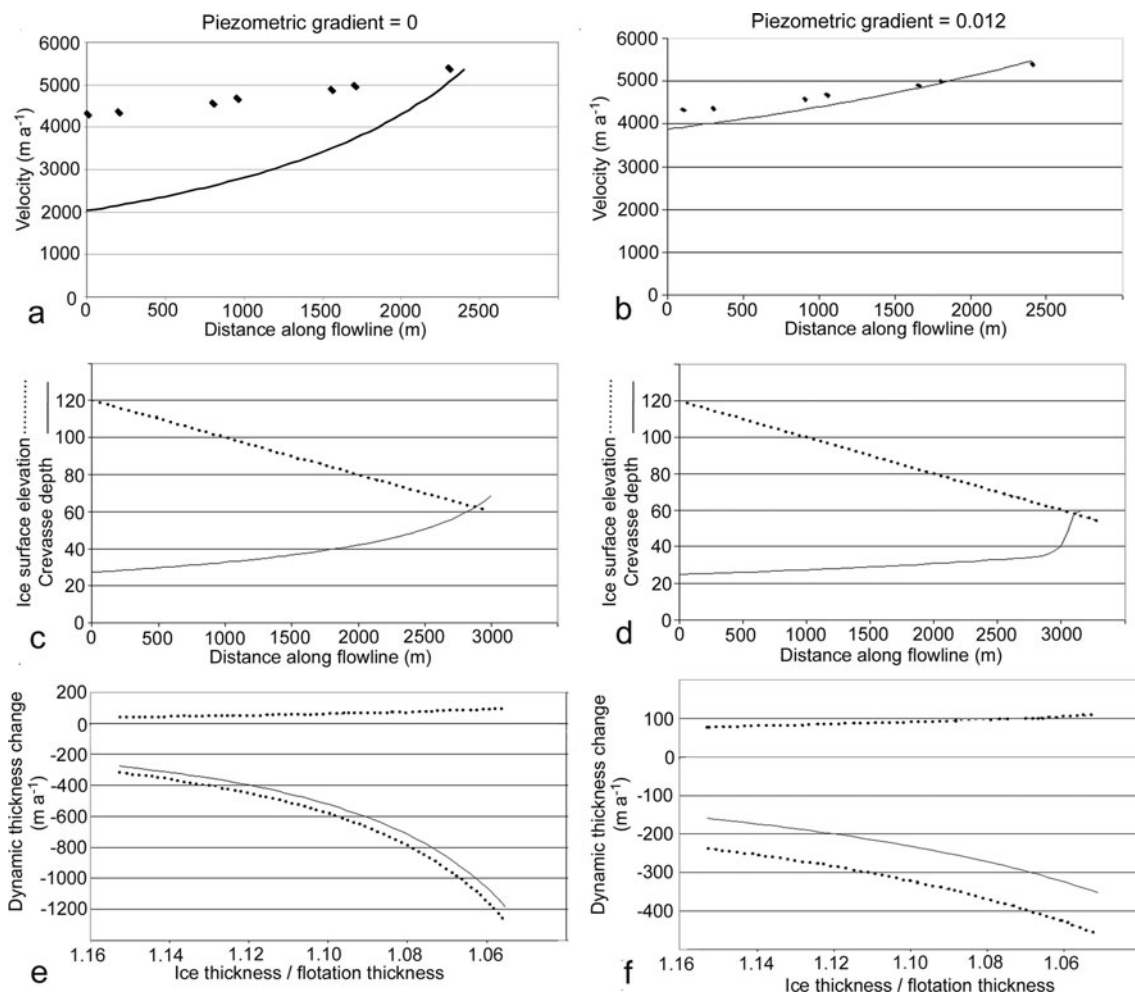


Fig. 5. Velocities (a, b), crevasse depths (c, d) and dynamic thinning rates (e, f) calculated from model 3, using the same input values as in Figure 4, assuming a horizontal piezometric surface (a, c, e), and a piezometric surface rising up-glacier (b, d, f).

widening will therefore result in higher ice velocities and longitudinal strain rates, increasing the likelihood that the calving margin will occur at such locations. Outlet glaciers and ice streams controlled by lateral drag should be insensitive to imposed thickness changes, and be relatively stable.

A new sliding function is proposed that parameterizes the effects of both lateral and basal drag. This model exhibits sensitivity to imposed thickness changes, but the stabilizing effects of lateral drag mean that the system will not necessarily exhibit dynamic instability as the glacier approaches flotation. Ice shelves will form where reduction of basal drag (and the corresponding flow acceleration and longitudinal strain rates) occurs over a sufficiently long spatial scale. This analysis yields significant new insights into the essential features of calving margins, which can be tested against new observations.

REFERENCES

- Alley, R.B., T.K. Dupont, B.R. Parizek and S. Anandkrishnan. 2005. Access of surface meltwater to beds of subfreezing glaciers: preliminary insights. *Ann. Glaciol.*, **40**, 8–14.
- Bindschadler, R. 1983. The importance of pressurized subglacial water in separation and sliding at the glacier bed. *J. Glaciol.*, **29**(101), 3–19.
- Brown, C.S., M.F. Meier and A. Post. 1982. Calving speed of Alaska tidewater glaciers, with application to Columbia Glacier. *USGS Prof. Pap.* 1258-C.
- Budd, W.F., P.L. Keage and N.A. Blundy. 1979. Empirical studies of ice sliding. *J. Glaciol.*, **23**(89), 157–170.
- Flowers, G.E. and G.K.C. Clarke. 2002. A multicomponent coupled model of glacier hydrology: 1. Theory and synthetic examples. *J. Geophys. Res.*, **107**(B11), 2287. (10.1029/2001JB001122.)
- Funk, M. and H. Röthlisberger. 1989. Forecasting the effects of a planned reservoir which will partially flood the tongue of Unteraargletscher in Switzerland. *Ann. Glaciol.*, **13**, 76–81.
- Haresign, E.C. 2004. Glacio-limnological interactions at lake-calving glaciers. (PhD thesis, University of St Andrews.)
- Hindmarsh, R.C.A. 2006. The role of membrane-like stresses in determining the stability and sensitivity of the Antarctic Ice Sheets: back pressure and grounding line motion. *Philos. Trans. R. Soc. London, Ser. A.*, **364**(1844), 1733–1767.
- Howat, I.M., I. Joughin, S. Tulaczyk and S. Gogineni. 2005. Rapid retreat and acceleration of Helheim Glacier, east Greenland. *Geophys. Res. Lett.*, **32**(22), L22502. (10.1029/2005GL024737.)
- Iken, A. and M. Truffer. 1997. The relationship between subglacial water pressure and velocity of Findelengletscher, Switzerland, during its advance and retreat. *J. Glaciol.*, **43**(144), 328–338.
- Krimmel, R.M. 2001. Photogrammetric data set, 1957–2000, and bathymetric measurements for Columbia Glacier, Alaska. *USGS Water-Resour. Invest. Rep.* 01-4089.
- Luckman, A. and T. Murray. 2005. Seasonal variations in velocity before retreat of Jacobshavn Isbræ, Greenland. *Geophys. Res. Lett.*, **32**(8), L08501. (10.1029/2005GL022519.)

- Marshall, S.J., D. Pollard, P.U. Clark and S.H. Hostetler. 2003. Coupling ice sheet and climate models for simulation of former ice sheets. In Gillespie, A., S.C. Porter and B.F. Atwater, eds. *The Quaternary period in the United States*. Amsterdam, Elsevier, 105–126.
- Meier, M.F. and A. Post. 1987. Fast tidewater glaciers. *J. Geophys. Res.*, **92**(B9), 9051–9058.
- Meier, M. and 9 others. 1994. Mechanical and hydrologic basis for the rapid motion of a large tidewater glacier. 1. Observations. *J. Geophys. Res.*, **99**(B8), 15,219–15,229.
- Nick, F.M. 2006. Modelling the behavior of tidewater glaciers. (PhD thesis, Utrecht University.)
- Nye, J.F. 1957. The distribution of stress and velocity in glaciers and ice-sheets. *Proc. R. Soc. London, Ser. A.*, **239**(1216), 113–133.
- O'Neel, S., K.A. Echelmeyer and R.J. Motyka. 2003. Short-term variations in calving of a tidewater glacier: LeConte Glacier, Alaska. *J. Glaciol.*, **49**(167), 587–598.
- Payne, A.J., A. Vieli, A. Shepherd, D.J. Wingham and E. Rignot. 2004. Recent dramatic thinning of largest West Antarctic ice stream triggered by oceans. *Geophys. Res. Lett.*, **31**(23), L23401. (10.1029/2004GL021284.)
- Raymond, C. 1996. Shear margins in glaciers and ice sheets. *J. Glaciol.*, **42**(140), 90–102.
- Raymond, C.F. and W.D. Harrison. 1987. Fit of ice motion models to observations from Variegated Glacier, Alaska. *IAHS Publ.* 170 (Symposium at Vancouver 1987 – *The Physical Basis of Ice Sheet Modelling*), 153–166.
- Rignot, E. and P. Kanagaratnam. 2006. Changes in the velocity structure of the Greenland Ice Sheet. *Science*, **311**(5673), 986–990.
- Rist, M.A. and 6 others. 1999. Experimental and theoretical fracture mechanics applied to Antarctic ice fracture and surface crevassing. *J. Geophys. Res.*, **104**(B2), 2973–2987.
- Robin, G.deQ. 1974. Correspondence. Depth of water-filled crevasses that are closely spaced. *J. Glaciol.*, **13**(69), 543.
- Sanderson, T.J.O. 1979. Equilibrium profile of ice shelves. *J. Glaciol.*, **22**(88), 435–460.
- Scambos, T.A., C. Hulbe, M. Fahnestock and J. Bohlander. 2000. The link between climate warming and break-up of ice shelves in the Antarctic Peninsula. *J. Glaciol.*, **46**(154), 516–530.
- Siegert, M.J. and J.A. Dowdeswell. 2004. Numerical reconstructions of the Eurasian Ice Sheet and climate during the Late Weichselian. *Quat. Sci. Rev.*, **23**(11–13), 1273–1283.
- Sikonia, W.G. 1982. Finite-element glacier dynamics model applied to Columbia Glacier, Alaska. *USGS Prof. Pap.* 1258-B.
- Smith, R.A. 1976. The application of fracture mechanics to the problem of crevasse penetration. *J. Glaciol.*, **17**(76), 223–228.
- Thomas, R.H., E.J. Rignot, K. Kanagaratnam, W.B. Krabill and G. Casassa. 2004. Force-perturbation analysis of Pine Island Glacier, Antarctica, suggests cause for recent acceleration. *Ann. Glaciol.*, **39**, 133–138.
- Van der Veen, C.J. 1996. Tidewater calving. *J. Glaciol.*, **42**(141), 375–385.
- Van der Veen, C.J. 1998a. Fracture mechanics approach to penetration of bottom crevasses on glaciers. *Cold Reg. Sci. Technol.*, **27**(3), 213–223.
- Van der Veen, C.J. 1998b. Fracture mechanics approach to penetration of surface crevasses on glaciers. *Cold Reg. Sci. Technol.*, **27**(1), 31–47.
- Van der Veen, C.J. 1999. *Fundamentals of glacier dynamics*. Rotterdam, A.A. Balkema.
- Van der Veen, C.J. 2002. Calving glaciers. *Progr. Phys. Geogr.*, **26**(1), 96–122.
- Van der Veen, C.J. and I.M. Whillans. 1989. Force budget: I. Theory and numerical methods. *J. Glaciol.*, **35**(119), 53–60.
- Van der Veen, C.J. and I.M. Whillans. 1996. Model experiments on the evolution and stability of ice streams. *Ann. Glaciol.*, **23**, 129–137.
- Vaughan, D.G. 1993. Relating the occurrence of crevasses to surface strain rates. *J. Glaciol.*, **39**(132), 255–266.
- Venteris, E.R. 1999. Rapid tidewater glacier retreat: a comparison between Columbia Glacier, Alaska and Patagonian calving glaciers. *Global Planet. Change*, **22**(1–4), 131–138.
- Vieli, A. and A.J. Payne. 2005. Assessing the ability of numerical ice sheet models to simulate grounding line migration. *J. Geophys. Res.*, **110**(F1), F01003. (10.1029/2004JF000202.)
- Vieli, A., M. Funk and H. Blatter. 2000. Tidewater glaciers: frontal flow acceleration and basal sliding. *Ann. Glaciol.*, **31**, 217–221.
- Vieli, A., M. Funk and H. Blatter. 2001. Flow dynamics of tidewater glaciers: a numerical modelling approach. *J. Glaciol.*, **47**(159), 595–606.
- Warren, C.R. 1992. Iceberg calving and the glacioclimatic record. *Progr. Phys. Geogr.*, **16**(3), 253–282.
- Weertman, J. 1979. The unsolved general glacier sliding problem. *J. Glaciol.*, **23**(89), 97–115.